Analysis of Quantum Machine Learning Algorithms in Noisy Channels for Classification Tasks in the IoT Extreme Environment

Sritam Kumar Satpathy, Vallabh Vibhu, Bikash K. Behera, Saif Al-Kuwari, Shahid Mumtaz and Ahmed Farouk

***Abstract*—By 2050, there will be a 50% rise in energy demand, and existing natural and renewable resources will be under extreme scrutiny. Optimizing current power generation and transmission to reduce energy consumption, cost, and other factors is equally vital to upgrading methods for effectively harvesting renewable energy. However, it gets more challenging for conventional computers to perform optimization as the number of factors affecting power generation and transmission rises. Extreme environmental cases will consequently lead to the imperfect functioning of IoT systems. By utilizing quantum-mechanical properties, such as superposition and entanglement, quantum computers can computationally outperform classical computers while consuming much less energy. In this paper, we investigate various quantum machine learning algorithms on two datasets (TWTDUS and SDWTT18) related to IoT extreme environment and study the effect of a noisy quantum environment. We observe that for the TWTDUS dataset, the variational $UU^\dagger$ with analytical clustering methods achieves the highest accuracy of 98.10%. Similarly, for the SDWTT18 dataset, the $UU^\dagger$ method with k-Means clustering achieves an accuracy of 94.43%. The results show that the accuracy of the proposed quantum algorithms outperforms the existing classical methods and can be utilized to forecast output power generation daily by measuring the metrics required in energy sector decision-making situations. This will be useful to save energy and costs in an IoT-extreme environment, where energy organizations must decide instantly whether to start or stop generating units.**

***Index Terms*—IoT Extreme Environment, Quantum Energy Utilization, Quantum Neural Network, $UU^\dagger$ Method, Variational $UU^\dagger$ Method**

I. Introduction

A. Quantum Computing and its Applications

Quantum computing uses quantum mechanical phenomena to perform computational tasks. The information is stored as quantum bits (qubits) and processed using unique quantum properties, such as superposition, entanglement, and interference [1]. Qubits require fewer resources than classical bits to store the same information. Indeed, quantum algorithms can solve some problems with lower time complexity than classical algorithms [2], [3], which have been realized by several *quantum supremacies* [4] (the demonstration of quantum computers solving problems that no classical computers can perform in a feasible time). Shor's factoring algorithm [5] and Grover's search algorithm [6] started a major move in quantum computing by demonstrating efficient quantum solutions to problems believed infeasible to solve. Since then, various applications of quantum computation have been realized, including artificial intelligence (AI) [7], quantum chemistry [8], financial modeling [9], drug discovery [10], weather forecasting [11], traffic optimization [12], intrusion detection [13], and modeling medical data [14].

B. Challenges in IoT Extreme Environments

According to the Energy Information Administration, global energy consumption is increasing by around 2.3% annually and is projected to surpass 700 quadrillions in 2040 [15]. The data required to manage power systems efficiently will grow rapidly in response to increasing global energy demand [16]. Despite being cost-free, renewable energy sources are unpredictable due to various factors, including variations in solar radiation, weather, and wind speed [17]. Internet of Things (IoT) systems are used for various applications, each with specific requirements and goals. IoT devices are particularly important and prioritized in various locations due to weak or deteriorating physical infrastructure, high demand, and extreme operating conditions caused by climate change. However, extreme weather, winds, flooding, storms, and other phenomena may affect the regular operation of specific infrastructure components and the employed IoT devices. In this environment, robustness/resilience scenarios that are typically neither random nor catastrophic but may experience varied degrees of area damage regularly are of relevance. Because of the growing demand for renewable energy, highly optimized energy management systems are required to identify the least expensive combination of all power generators (conventional and renewable) and storage capacity that can meet the anticipated demand with the bare minimum of security. Finding the ideal balance between dependability, availability, efficiency, and cost requires optimization strategies to support the net-

S. K. Satpathy is with the Department of Physical Sciences, Indian Institute of Science Education and Research, Berhampur, India e-mail: (sritamkumar04@gmail.com).

V. Vibhu is with the Department of Physical Sciences, Indian Institute of Science Education and Research, Berhampur, India e-mail: (vallabhvibhu07@gmail.com).

B. K. Behera is with the Bikash's Quantum (OPC) Pvt. Ltd., Mohanpur, WB, 741246 India, e-mail: (bikas.riki@gmail.com).

Saif Al-Kuwari is with the College of Science and Engineering, Hamad Bin Khalifa University, Qatar Foundation, Doha, Qatar. e-mail: (smalkuwari@hbku.edu.qa).

Shahid Mumtaz is with the Department of Applied Informatics Silesian University of Technology Akademicka 16 44-100 Gliwice, Poland, and Nottingham Trent University, Engineering Department, United Kingdom. e-mail: (dr.shahid.mumtaz@ieee.org).

A. Farouk is with the Department of Computer Science, Faculty of Computers and Artificial Intelligence, South Valley University, Hurghada, Egypt. e-mail: (ahmed.farouk@sci.svu.edu.eg).

work or "smart grid" function [18]. Unfortunately, large processing power is required to accomplish such optimization on a large scale [19], including power generation, transmission, and distribution [20]. For example, optimizing a shale-gas supply chain network that spans 10,000 km^2 may require more than 50k variables and 50k constraints. Modern supercomputers may sometimes take many days or more than 15 hours to generate a solution [21]. The high computational cost limits the effectiveness of national and worldwide energy system optimization.

C. Quantum solutions

In addition to delivering a crucial speed advantage over traditional computers, quantum computing offers a new strategy for tackling some of the most challenging issues [22]. Energy resources, including power grid location, wind turbine placement, transmission costs, solar panel alignment, and other factors must be optimized to reduce energy waste, capital, and operational costs. The computation time required to find a solution increases exponentially with more power-producing facilities [23]. For the energy sector, quantum simulation and energy system optimization are the most beneficial in providing workable solutions with reasonable runtime for such energy system optimization challenges [24]. For example, a single-core CPU takes almost 11 hours to solve a simulation problem to find the best location for 14 facilities compared to 16 minutes on a quantum processor [25].

Unit commitment is another optimization problem for applying quantum computation [26]. A typical power company runs hundreds or thousands of generation units with distinct costs and capacities, continuously changing the need for power. Companies must make instantaneous decisions about turning on or off generation units based on a variety of factors, including fixed and variable costs, grid and unit constraints, load forecasts, heat rate curves, and sustainability considerations, to meet power demand while minimizing operating costs [27]. The growth of generation units makes traditional computing-based decision-making methods ineffective. Recently, Microsoft has shown its quantum-inspired unit commitment algorithm, which operates significantly more quickly than traditional solvers [28]. In particular, Microsoft researchers found the required cofactor chemical to simulate the complex Haber process, which does not apply to classical computers [29]. However, the quantum advancement of Haber is still about ten years away. Similarly, quantum computing has been used by many industries, such as Mitsubishi, to develop battery technology [30] and NASA to organize a series of high-battery-power actions carried out by planetary explorers to achieve mission objectives [31].

Clustering is another potential application of quantum computing in the energy sector, which divides the data points into subgroups based on their similarity. It is often defined by the Euclidean distance between points in m-dimensional space. Furthermore, classification can be defined by such clustering, which can assist in creating focused models for predicting future outcomes within each subgroup. However, it is NP-hard to compute the partitioning of n data points into k clusters since there are k^n possible partitioning options and this number grows exponentially with n [32]. Instead, oftentimes, a heuristic approach is adopted, where algorithms, such as k-Means, discover local minimum solutions but could overlook subtle and significant similarities, which improve categorization and the accuracy of ensuing model predictions.

The contributions of this paper can be summarized as follows:

- Various quantum machine learning methods, namely $UU^\dagger$, variational $UU^\dagger$ and quantum neural networks are applied to perform binary classification of two power generation datasets (TWTDUS and SDWTT18) related to IoT extreme environment.
- Two types of clustering, named k-Means and Analytical methods, are used to cluster the datasets for the $UU^\dagger$ and variational $UU^\dagger$ methods.
- The robustness of the algorithms is checked in the presence of different noisy channels such as bit-flip, phase-flip, amplitude damping, phase damping and depolarizing.

D. Organization

The rest of the paper is organized as follows. Section II discusses related works, followed by Section III, where the methodology of the algorithms is described. In Section IV, the results are presented and discussed with the given datasets. Finally, Section V discusses the results and provides a few concluding remarks as well as suggestions for extensions to this work.

II. Related Work

Clustering and nearest-neighbor algorithms have been investigated and tested on adiabatic quantum computers [33], [34], which are based on minimizing the energies of Ising models [35]. In this case, a clustering problem is transferred to a quadratic unconstrained binary optimization (QUBO) problem and utilized for pattern recognition and binary classification [36]. Instead, new quantum algorithms, such as quantum collaborative k-Means [37] and q-means [38] are proposed for unsupervised learning. The enhancement of the encoding approach to perform the required function adequately on an IBM quantum computer is investigated in [39]. Similarly, achieving data categorization by employing a nearest-neighbor classification and providing an optimal technique for encoding 8-dimensional classical data into the quantum computer using the IonQ quantum hardware is demonstrated in [40]. A generalized quantum k-Means clustering and popular swap-test-based distance estimation approaches for classification and clustering are explored in [41], which demonstrates how clustering might be used to classify energy grids.

IoT deployment has become a collaborative effort, and its integration provides new opportunities to investigate contemporary challenges in IoT systems from various perspectives. However, due to the distributed nature of IoT devices, which present a vast and vulnerable surface, this integration introduces new challenges. Therefore, the current IoT architecture must undergo changes and improvements to enable an effective operation and meet the needs of the IoT ecosystem. Quantum

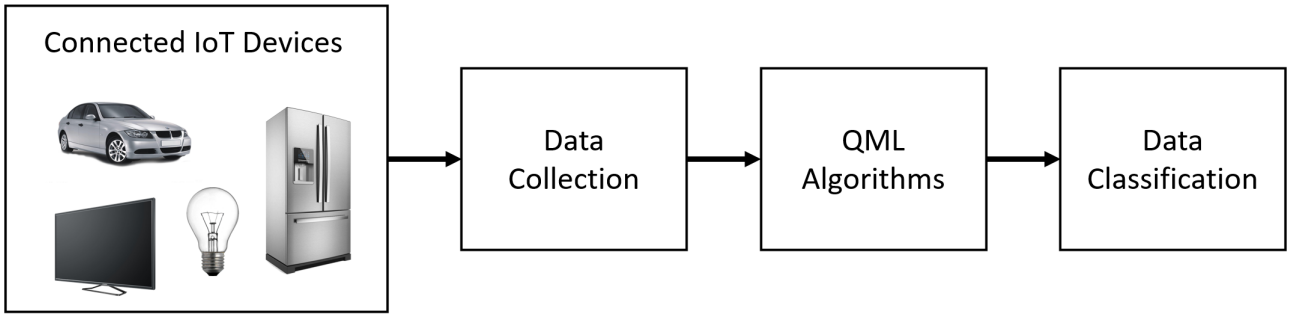

Fig. 1: Quantum Machine Learning for IoT System.

machine learning (QML) is one of the most potent data exploration approaches for understanding regular interaction patterns and performing tasks such as classification or prediction, which can outperform classical techniques. IoT system architecture employing a QML technique is shown in Fig. 1. The schematic diagram provides a general overview of collecting data and applying QML algorithms for data classification. In the first step, IoT chips connected to appliances like refrigerators, cars, bulbs, etc., measure and store data retrieved from IoT devices and analyzed. After that, quantum machine learning algorithms can be applied to perform classification tasks on this data.

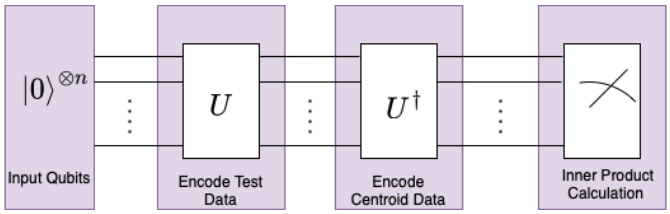

(a)

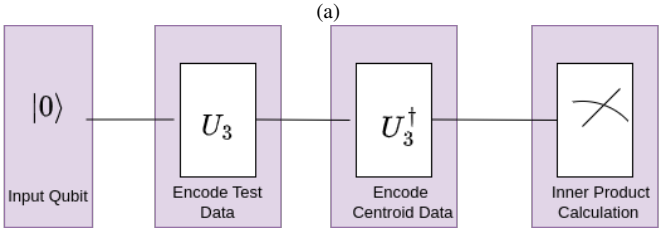

(b)

Fig. 2: (a) Generalized circuit for $UU^\dagger$ methodology. The qubits are prepared in $|0\rangle^{\otimes n}$ state. A general n-qubit unitary gate is used to encode the testing data, and its dagger is applied to encode the centroid data. In the end, measurement is performed, and the inner product between the centroid and testing data is calculated. (b) An example circuit for our dataset, where one feature is used for the classification. U_3 is used, where the data feature values are encoded in angles of $U_3(\theta, 0, 0)$ gate, and the analytic cluster centers are added in $U^\dagger(-\theta, 0, 0)$ gate. Finally, the inner product is calculated by measuring the quantum circuit.

III. Methodology

This section proposes the working principles of various clustering methods such as analytical, k-Means, and classification algorithms like $UU^\dagger$, variational $UU^\dagger$, and quantum

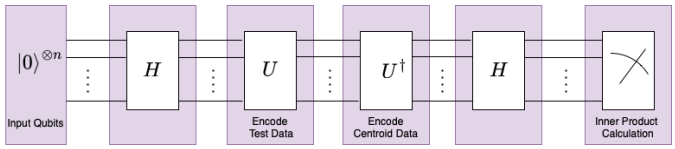

(a)

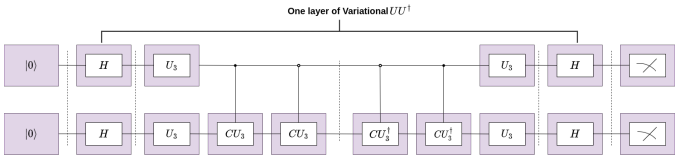

(b)

Fig. 3: (a) Generalized quantum circuit for the variational $UU^\dagger$ method. One layer is given by applying a Hadamard, U gate, and their inverse form the whole circuit. (b) An example circuit for our TWTDUS dataset consists of four data features encoded in angles and added into two $U_3(\theta, 0, 0)$, and two controlled U_3 gates. While the cluster centers for respective data features are added in two anti-controlled $U_3^\dagger$, and two $U_3^\dagger(\theta, 0, 0)$ gates. To make n layers, the structure of (HU) will be repeated n times, and then $(U^\dagger H)$ will be repeated n times.. The inner product between the testing data and centroid data is calculated from the measurement of the quantum circuit.

neural network. Also, the noisy environment's effect on these algorithms has been demonstrated.

A. Clustering Methods

1) Analytical

We designed a clustering algorithm for our datasets, namely analytical clustering, in which the power generation will be divided into two groups based on the behavior of power generation dependencies on various features. The analytical clustering method computes the average of the generated power of a dataset's maximum and minimum values. It divides the dataset into two groups based on the closest value to the average, saying a (above a in one group and below a in another group). The characteristics responsible for power generation, such as wind speed, wind direction, pressure, temperature, etc., correspond to a, are extracted, and the cluster's centroid is selected. One of the cluster centers is the nearest value to the average sum of the previously obtained feature values and the minimal value of the feature in the dataset. At the same time,

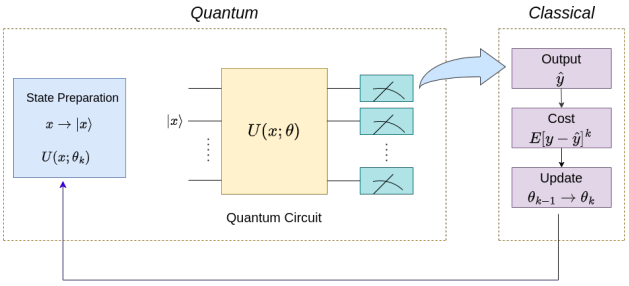

Fig. 4: The variational circuit model. First, the quantum state $|x\rangle$ is prepared by preprocessing all the input data x on a classical device. Then, the quantum hardware computes the unitary operation with the quantum state $|x\rangle$ along with variational parameters θ. This unitary operation is evolved to achieve the expected output. After measurement, the cost function is calculated and the variational parameter θ is updated to minimize the cost function. After that, the state $|x\rangle$ along with the updated variational parameters θ passed to a unitary operation, and the process is repeated until the minimum cost function is achieved. The output corresponding to the minimum cost function provides the solution to the required problem.

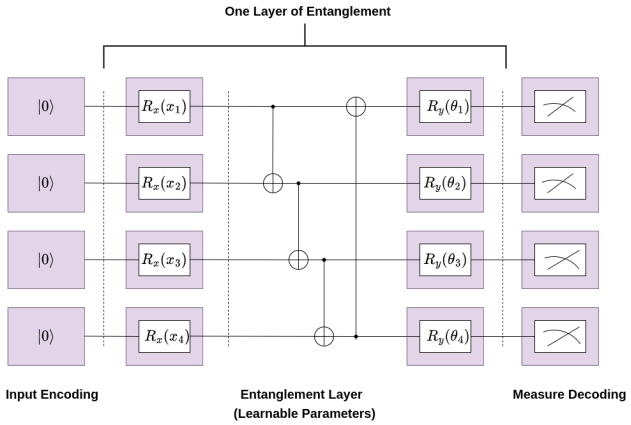

Fig. 5: Circuit of QNN with the input $|x\rangle$. The qubits are initialized in the $|0000\rangle$ state, the data is encoded and an entanglement layer is applied. After measurement, the loss function and accuracy are calculated.

the other one is the nearest value to the average sum of this feature value and its maximum value in the dataset. The two values of cluster centers are fitted into the $U^\dagger$ with the test data values encoded into the U to calculate the inner product. The test data value is assigned to the cluster center with the highest inner product value.

2) k-Means

k-Means clustering is an unsupervised learning approach that separates a dataset into many groups. Here, k represents the number of clusters into which the dataset must be divided. Without training, it enables us to divide a dataset into clusters where each cluster has a centroid. The primary goal is to reduce the sum of the total distance between each data point and its matching cluster. It begins by dividing the dataset into clusters based on the value k and repeats the procedure until obtaining the optimal cluster. In this paper, our dataset is clustered using the k-Means technique with $k = 2$, and the quantum circuit is built after observing the two centroids of each column in the dataset.

Algorithm 1: $UU^\dagger$ classification algorithm.

Input All the features of the dataset and their centroids
Output Accuracy of the classification
Construct the circuit with n-qubit unitary operation U and n-qubit $U^\dagger$ operation
Encode the testing data in the U operator, resulting in the state $|\phi_i\rangle$, and the centroid data in the $U^\dagger$ operator, resulting in $|\psi_1\rangle$and $|\psi_2\rangle$ representing cluster 1 and 0.
Measure the quantum circuit with the first centroid data and then with the second centroid data
If $\langle\phi_i|\psi_1\rangle > \langle\phi_i|\psi_2\rangle$, **then** corresponding training data $\in$ cluster - 1
Else corresponding centroid data $\in$ cluster - 0
EndIf
Compare the result with analytical clustering/ k-Means clustering
If c number of correct matching of cluster found with analytical clustering/ k-Means clustering, then calculate the accuracy using the relation

$$\frac{c}{\text{Total number of data}} \times 100$$

Algorithm 2: Variational $UU^\dagger$ classification algorithm for m layers.

Input All the features of the data and their centroids ;
Output Accuracy of the classification;
for $m \in \mathbb{N}$ **do**
    Construct the circuit containing n Hadamard gates, n-qubit unitary operation U, and the dagger of all gates sequentially ;
Encode the testing data in the U operator, resulting in the state $|\phi_i\rangle$, and the centroid data in the $U^\dagger$ operator, resulting in $|\psi_1\rangle$and $|\psi_2\rangle$ representing cluster 1 and 0. ;
Measure the quantum circuit with the first centroid data and then with the second centroid data;
If $\langle\phi_i|\psi_1\rangle > \langle\phi_i|\psi_2\rangle$;
then corresponding centroid data $\in$ cluster - 1;
Else corresponding centroid data $\in$ cluster - 0 ;
EndIf ;
Compare the result with analytical clustering/ k-Means clustering ;
If c number of correct matching of clusters found with the analytical clustering/ k-Means clustering, then calculate the accuracy using the relation ;

$$\frac{c}{\text{Total number of data}} \times 100$$

B. Classification Methods

1) $UU^\dagger$ Classification

In this classification technique, the circuit is built after selecting the centroid of each column either using Analytical or k-Means clustering. In the quantum circuit (generalized Fig. 2a), two U_3 gates are applied to each of the two qubits, followed by a controlled U_3 gate and an anti-controlled U_3 gate. Data for each of the four characteristics were encoded into the four gates, and the corresponding centroid of the data value in their dagger is the mirror image of each gate. The k-Means clustering method creates two centers; as a result, the four dagger gates encode the initial centroid of each factor involved in power production, and the associated U gates encode all data characteristics that were calibrated to angle

value between 0 and π (i.e., wind speed and wind direction in two U_3 gates, pressure in CU_3 gate and air temperature in CU_3 gate). Accordingly, the probability of $|00\rangle$ is calculated, and similarly, the second centroid of each factor was encoded in every gate's dagger. If the probability ($|00\rangle$) using the first centroid is greater than the probability ($|00\rangle$) using the second centroid, then the encoded test data belongs to the first cluster; otherwise, it belongs to the second cluster. The $UU^\dagger$ method of classification using k-Means clustering is applied for the TWTDUS dataset. However, in the SDWTT18 dataset, only two features contribute to the low voltage (LV) active power. The two features are placed in the θ values of two U_3 gates and their centroids in the two $U_3^\dagger$ gates, which are identical mirror copies of the two U_3 gates. Here, the state $|\phi_i\rangle$ is prepared using the U gate. Similarly, $|\psi_1\rangle$ and $|\psi_2\rangle$ $\rangle$ states are prepared using $U^\dagger$ gate. After that, measurement is done, the inner product between $|\phi_i\rangle$ and $|\psi_1\rangle$, and between $|\phi_i\rangle$ and $|\psi_2\rangle$ is calculated. If $\langle\phi_i|\psi_1\rangle > \langle\phi_i|\psi_2\rangle$, the data point belongs to cluster 1, otherwise cluster 0, as shown in Algorithm 1. The required steps, generalized, and an example circuit for analytical clustering are presented in Fig. 2a and Fig. 2b respectively.

2) Variational $UU^\dagger$ Classification

Variational $UU^\dagger$ classification follows the same process as the $UU^\dagger$ method, except the Hadamard gate is placed after $|0\rangle$ state and just before the measurement box. The circuit consists of equally repeating layers of (HU) and $(U^\dagger H)$ gates. The variational $UU^\dagger$ circuit for one layer is shown in Fig. 3b. To increase the layering of the circuit, (HU) operation for n number of times followed by $(U^\dagger H)$ are applied. Then, the measurements are performed, and the probability of $|00\rangle$ is calculated. If the probability ($|00\rangle$) using the first centroid is greater than that using the second centroid, the data belongs to the first cluster; otherwise, it belongs to the second cluster. After that, the two clusters are compared with the k-Means clustering, and the accuracy is calculated using the beforementioned techniques ($UU^\dagger$ classification). If $\langle\phi_i|\psi_1\rangle > \langle\phi_i|\psi_2\rangle$ then the data point belongs to the cluster 1, otherwise 0, as shown in algorithm 2 and its generalized quantum circuit in Fig. 3a.

C. Quantum Neural Network

1) Variational Quantum Circuits

A variational quantum circuit (VQC) [42] is a quantum circuit that has several rotation operator gates to perform various numerical tasks such as classification, optimization, and approximation. The algorithm utilized in the VQC is known as the variational quantum algorithm and is a classical-quantum hybrid algorithm since a classical computer conducts its parameter optimization. It approximates function by parameter learning; hence it is comparable to an artificial neural network but differs owing to many quantum computing characteristics. Entanglement layers (Fig. 5), rather than activation functions, are used to create multilayer structures in quantum neural networks since quantum gate operations are reversible linear processes. The rotation angles of some quantum gates are used to encode the variational parameters in VQC, which are present in the form of quantum circuits. The parameterized single-qubit rotation gates ($R_x(\theta), R_y(\theta)$ and $R_z(\theta)$), controlled-Not gates, and controlled-Z gates are the most often used quantum gates.

$$
\begin{aligned}
R_y(\theta) &= \begin{bmatrix} \cos\theta & -\sin\theta \\ \sin\theta & \cos\theta \end{bmatrix}, \\
CNOT &= \begin{bmatrix} 1 & 0 & 0 & 0 \\ 0 & 1 & 0 & 0 \\ 0 & 0 & 0 & 1 \\ 0 & 0 & 1 & 0 \end{bmatrix}, \\
CZ &= \begin{bmatrix} 1 & 0 & 0 & 0 \\ 0 & 1 & 0 & 0 \\ 0 & 0 & 1 & 0 \\ 0 & 0 & 0 & -1 \end{bmatrix}
\end{aligned} \tag{1}
$$

The parameterized quantum circuit $U(x, \theta)$ [43], the quantum output $\hat{y}$, and the updating method for the parameter θ comprise the variational circuit's three basic components. The data, x, is first preprocessed on a classical device to identify the quantum input state. Then, using randomly initialized parameters θ, the quantum hardware computes $U(x; \theta)$ with a quantum state $|x\rangle$. The classical component analyzes the measurements following several $U(x; \theta_k)$ executions and produces a prediction, $\hat{y}$. The parameters are updated in a closed loop between the classical and quantum hardware, and the entire cycle is repeated several times.

2) Cost function

In machine learning, the loss function [43] calculates the difference between the actual and predicted value and measures how well the machine learning model performs. The loss function is calculated as follows:

$$\text{loss} = (\hat{y}_i - y_i)^2 \tag{2}$$

where $\hat{y}$ is the predicted value and y is the actual value.

A loss function is produced for the complete training dataset, and its average is known as the cost function C. The below cost function is also known as mean square error (MSE).

$$C = \frac{1}{n}\sum_{i=1}^{n}(\hat{y}_i - y)^2 \tag{3}$$

3) Back propagation with Gradient Descent

The update rule for weights in QNN is given by

$$\theta_i = \theta_i - \eta\frac{\partial C}{\partial \theta_i} \tag{4}$$

The chain rule can be used to find the partial derivative. The detailed procedure is given in algorithm 3 and Fig. 4.

D. Noise Models

We adopt five different forms of noise models: bit-flip, phase-flip, amplitude-damping, phase-damping, and depolarizing noise are discussed [44].

1) Bit-flip noise model

In bit-flip noise, the quantum state $|0\rangle$ is changed to $|1\rangle$ and the quantum state $|1\rangle$ is changed to $|0\rangle$. The probability of a state change is η_B, while the probability that it stays the same is $(1-\eta_B)$. The operations of this model on qubits are characterized by the Kraus operators, which are provided by:

$$\begin{aligned} E_0^B &= \sqrt{1-\eta_B}\ \mathbb{I} = \sqrt{1-\eta_B}\begin{bmatrix}1 & 0\\ 0 & 1\end{bmatrix} \\ E_1^B &= \sqrt{1-\eta_B}\ \mathbb{X} = \sqrt{\eta_B}\begin{bmatrix}0 & 1\\ 1 & 0\end{bmatrix} \end{aligned}$$

where $0 \leq \eta_B \leq 1$ represents the bit-flip error probability, which indicates the probability of an error happening in the quantum state as a result of a transferred qubit.

2) Phase-flip noise model

When phase-flip noise occurs, the qubit's phase shifts from $|1\rangle$ to -$|1\rangle$ and stays the same if the qubit is in $|0\rangle$. The Kraus operators of the Phase-flip noise model are provided by:

$$\begin{aligned} E_0^P &= \sqrt{1-\eta_P}\mathbb{I} = \sqrt{1-\eta_P}\begin{bmatrix}1 & 0\\ 0 & 1\end{bmatrix} \\ E_1^P &= \sqrt{\eta_P}\mathbb{Z} = \sqrt{\eta_P}\begin{bmatrix}1 & 0\\ 0 & -1\end{bmatrix} \end{aligned}$$

where $0 \leq \eta_P \leq 1$ represents the bit-flip error probability, which indicates the probability of an error happening in the quantum state as a result of a transferred qubit.

3) Amplitude damping noise model

In many different quantum systems, the amplitude damping process is crucial for predicting energy dissipation, and the following matrices give their Kraus operators,

$$\begin{aligned} E_0^A &= \begin{bmatrix}1 & 0\\ 0 & \sqrt{1-\eta_A}\end{bmatrix} \\ E_1^A &= \begin{bmatrix}0 & \sqrt{\eta_A}\\ 0 & 0\end{bmatrix} \end{aligned} \tag{5}$$

where the decoherence rate of amplitude damping is given by $0 \leq \eta_A \leq 1$, which indicates the possibility of occurring an error in the quantum state as a result of a travel qubit.

4) Phase damping noise model

This noise model loses relative phase information about a quantum state. The Kraus operators for this noise are given by,

$$\begin{aligned} E_0^P &= \sqrt{1-\eta_P}\begin{bmatrix}1 & 0\\ 0 & 1\end{bmatrix} \\ E_1^P &= \begin{bmatrix}\sqrt{\eta_P} & 0\\ 0 & 0\end{bmatrix} \\ E_2^P &= \begin{bmatrix}0 & 0\\ 0 & \sqrt{\eta_P}\end{bmatrix} \end{aligned} \tag{6}$$

where the decoherence rate of the phase damping is given by $0 \leq \eta_P \leq 1$, which indicates the possibility of occurring an error in the quantum state as a result of a transferred qubit.

5) Depolarising noise model

In a depolarising noise model, the likelihood that the quantum state's qubits will get depolarized in a noisy environment is η_D, while the probability that they will remain invariant is $1-\eta_D$. The probability of the Pauli operators $\mathbb{X}$, $\mathbb{Y}$, and $\mathbb{Z}$ acting on the qubits is $\eta_D/3$. The following matrices give the Kraus operators

$$\begin{aligned} E_0^D &= \sqrt{1-\eta_D}\begin{bmatrix}1 & 0\\ 0 & 1\end{bmatrix} \\ E_1^D &= \frac{\eta_D}{3}\begin{bmatrix}0 & 1\\ 1 & 0\end{bmatrix} \\ E_2^D &= \frac{\eta_D}{3}\begin{bmatrix}0 & -i\\ i & 0\end{bmatrix} \\ E_3^D &= \frac{\eta_D}{3}\begin{bmatrix}1 & 0\\ 0 & -1\end{bmatrix} \end{aligned} \tag{7}$$

Algorithm 3: Algorithm for quantum neural network method for m hidden layers.

Input All the features of the data ;
Output Accuracy of the classification;
Initialize all the qubits in $|0\rangle^{\otimes n}$ state ;
for $m \in \mathbb{N}$ **do**
  Construct the circuit containing n R_x gates. Add one hidden layer with n $CNOT$ gates and n $R_y(\theta_i)$ gates for $i = 0, 1, 2...., n-1$, where n is the number of features used for classification. Similarly, add m hidden layers. ;
Convert all the feature values from 0 to π. ;
Use analytical clustering 1 and 0 for target data.;
Encode the four features of the data in the θ position of four R_x operators, respectively;
Measure the quantum circuit, calculate the loss function, update the weights and calculate the accuracy. ;

IV. Experimental Results

To evaluate the models, the IBM Qasm simulator is used to run the circuit by employing 8192 shots to take measurements for calculating the accuracy of $UU^\dagger$ and variational $UU^\dagger$. In comparison, 10,000 shots are used for QNN. In this section, the results of our evaluations are presented.

A. Dataset

In this paper, we evaluate our models on two datasets: TWTDUS and SDWTT18.

1) TWTDUS Dataset

This dataset contains the hourly time-series dataset for Texas, US, across an entire year and was generated by National Renewable Energy Laboratory (NREL) software named Texas Wind Turbine Dataset, US (TWTDUS). It has 8760 rows and 5 columns describing various weather properties that may be categorized using different QML approaches. Sample records and their detailed statistics from the TWTDUS dataset are shown in Tables I and II, respectively. The system power generation versus all the features for the original dataset without clustering is shown in Fig. 6. It is evident that the relation of power generated to wind speed is linear, while the other graphs do not state any strong relationship between the features and power generation.

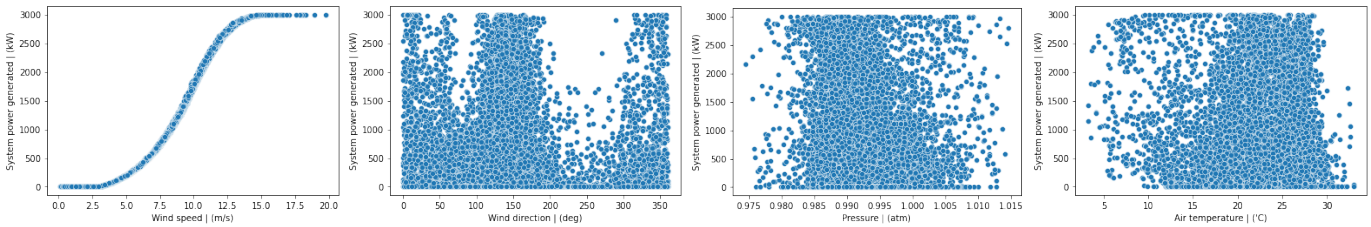

(a) Power vs Wind Speed (b) Power vs Wind Direction (c) Power vs Pressure (d) Power vs Air Temperature

Fig. 6: The relation of the generated power of the TWTDUS dataset without clustering against (a) Wind Speed, (b) Wind Direction, (c) Pressure, and (d) Air Temperature.

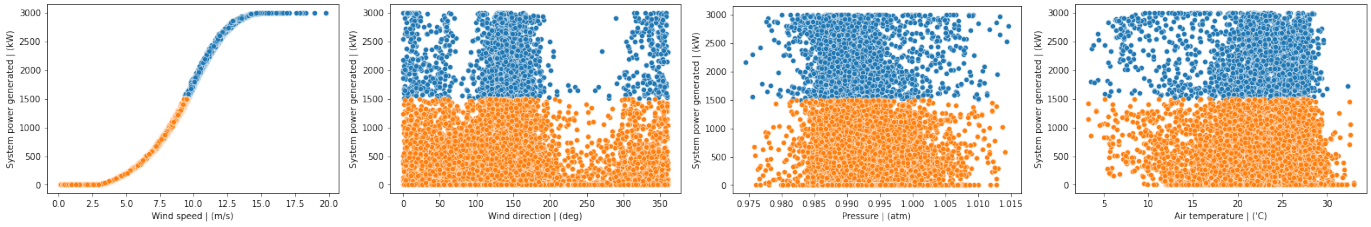

(a) Power vs. Wind Speed (b) Power vs. Wind Direction (c) Power vs. Pressure (d) Power vs. Air Temperature

Fig. 7: The relation of the generated power above 1501.66 KW and below 1501.66 KW with analytical clustering for the TWTDUS dataset against (a) Wind Speed, (b) Wind Direction, (c) Pressure, and (d) Air Temperature.

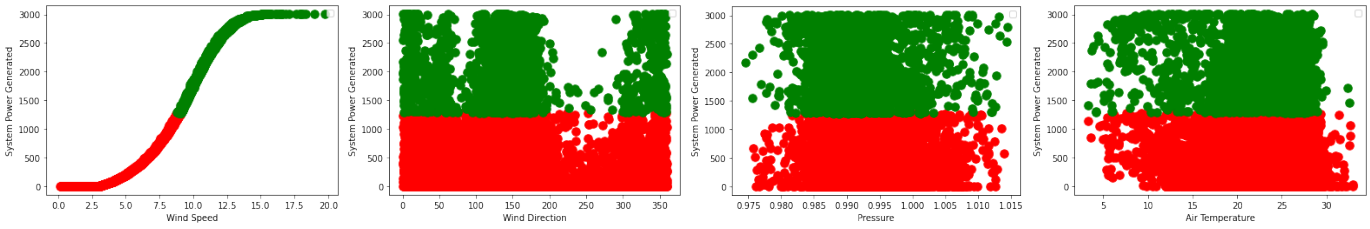

(a) Power vs Wind Speed (b) Power vs Wind Direction (c) Power vs Pressure (d) Power vs Air Temperature

Fig. 8: The relation of the generated power with k-Means clustering for the TWTDUS dataset against (a) Wind speed, (b) Wind Direction, (c) Pressure, and (d) Air Temperature. The red and green dots indicate the two clusters to which every dataset has been assigned.

Time stamp	System power generated | (kW)	Wind speed | (m/s)	Wind direction | (deg)	Pressure | (atm)	Air temperature| (°C)
Jan 1, 12:00 am	1766.64	9.926	128	1.000480	18.263
Jan 1, 01:00 am	1433.83	9.273	135	0.999790	18.363
Jan 1, 02:00 am	1167.23	8.660	142	0.999592	18.663
Jan 1, 03:00 am	1524.59	9.461	148	0.998309	18.763
Jan 1, 04:00 am	1384.28	9.184	150	0.998507	18.963

TABLE I: A sample of the TWTDUS dataset.

2) SDWTT18 Dataset

The data in this dataset was acquired from a wind turbine Scada system that operated and generated power in Turkey, named the 2018 Scada Data of a Wind Turbine in Turkey (SDWTT18). The SCADA system measures various features like wind speed, wind direction, generated power, etc., in 10-minute intervals. It contains 50530 rows and 4 columns. Sample records and their detailed statistics from the SDWTT18 dataset are shown in Tables III and IV respectively.

B. Clustering

1) TWTDUS Dataset

The dataset includes five columns: timestamps, system power generated, wind speed, wind direction, and pressure. We aim to classify the generated power based on factors contributing to power generation, such as wind speed, wind direction, pressure, and air temperature. The generated power by the system is divided into two categories: above 1501.66 KW and below 1501.66 KW, where 1501.66 KW is the closest average power value. The generated system power versus wind speed increases linearly in the case of clustering by the analytical method. However, the generated system power versus other factors cannot draw any conclusions while fluctuating, as shown in Fig. 7, so they are not classified according to the $UU^{\dagger}$ classification method. Fig. 8 demonstrates that generated system power of a value lower than 1500 and greater than 1000 has become the barrier that separates the two clusters when applying the k-Means clustering method.

Features	Counts	Mean	std	min	max
system power generated (kw)	8760.000000	964.467934	878.558112	0.000000	3004.010000
Wind speed (m/s)	8760.000000	7.376120	3.138291	0.119000	19.743000
Wind direction (deg)	8760.000000	146.616210	84.678754	0.000000	360.000000
Pressure (atm)	8760.000000	0.992368	0.005332	0.974514	1.014510
Air temperature ($^{\circ}C$)	8760.000000	22.147298	4.855232	3.263000	32.963000

TABLE II: Statistics of the TWTDUS dataset.

Date/Time	LV Active Power | (kW)	Wind Speed | (m/s)	Theoretical Power Curve | (KWh)	Wind Direction | ()
01 01 2018 00:00	380.047791	5.311336	416.328908	259.994904
01 01 2018 00:10	453.769196	5.672167	519.917511	268.641113
01 01 2018 00:20	306.376587	5.216037	390.900016	272.564789
01 01 2018 00:30	419.645905	5.659674	516.127569	271.258087
01 01 2018 00:40	380.650696	5.577941	491.702972	265.674286

TABLE III: A sample of the SDWTT18 dataset.

Features	Counts	Mean	std	min	max
LV Active Power (kW)	50530.000000	1307.684332	1312.459242	-2.471405	3618.732910
Wind Speed (m/s)	50530.000000	7.557952	4.227166	0.000000	25.206011
Theoretical Power Curve (KWh)	50530.000000	1492.175463	1368.018238	0.000000	3600.000000
Wind Direction ()	50530.000000	123.687559	93.443736	0.000000	359.997589

TABLE IV: Statistics of the SDWTT18 dataset.

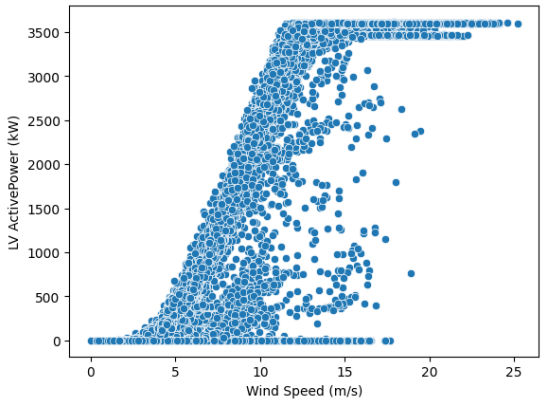

(a) Power vs Wind Speed

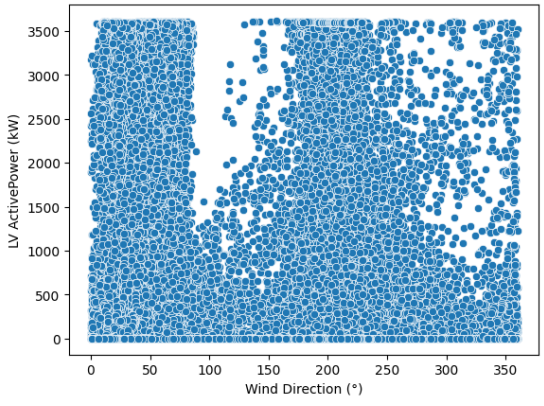

(b) Power vs Wind Direction

Fig. 9: The relation of the generated power without clustering for the SDWTT18 dataset against (a) Wind speed and (b) Wind direction.

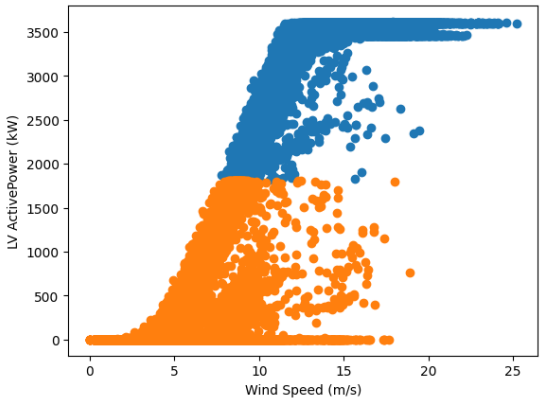

(a) Power vs Wind Speed

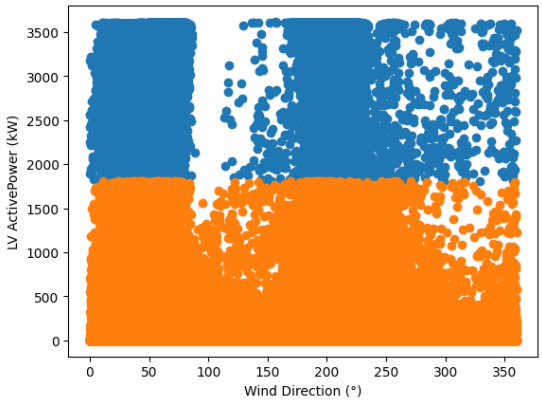

(b) Power vs Wind Direction

Fig. 10: The relation of the generated power above 1808.30895996093 KW and below 1808.30895996093 KW with analytical clustering for the SDWTT18 dataset against (a) Wind Speed and (b) Wind Direction.

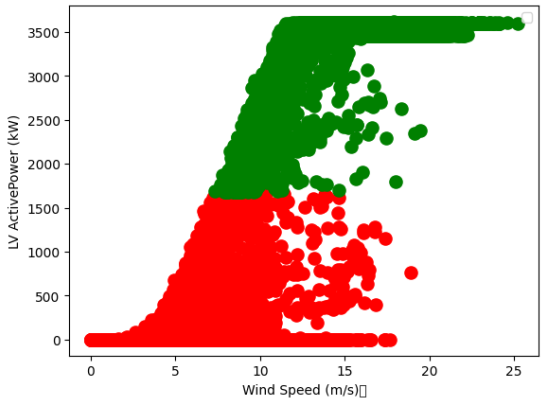

(a) Power vs Wind Speed

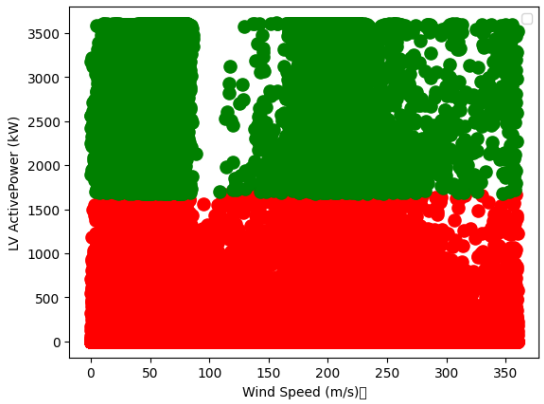

(b) Power vs Wind Direction

Fig. 11: The relation of the generated power with k-Means clustering for the SDWTT18 dataset against (a) Wind speed and (b) Wind Direction. The red and green dots indicate the two clusters to which every dataset has been assigned.

2) SDWTT18 Dataset

The dataset contains five columns: date/time, LV active power, wind speed, theoretical power curve, and wind direction. The main goal is to classify the dataset based on the features contributing to the LV active power. The LV active power versus wind speed curve shows an almost linear dependency, as shown in Fig. 9, and this feature will be only considered for $UU^\dagger$ classification. The average value of LV active power's minimum and maximum values is calculated, and the nearest point to that value is chosen, which is 1808.30895996093. Therefore, the LV active power is split into two categories: over and below 1808.30895996093. The clustering using analytical and k-Means is shown in Fig. 10 and 11 respectively.

C. Classification Techniques

1) $UU^\dagger$ classification

In this classification, the centroid point for each feature responsible for power generation is chosen, the total data values for each factor are mapped from 0 to π and encoded into the θ of the U gate, and the ϕ and λ values are set to zero. A $U^\dagger$ unitary operator is created with parameters $(\theta, 0, 0, 0)$ using the previously defined centroid, and various θ valued U unitary operators are created from the encoded data corresponding to each θ value. A quantum circuit is created to measure the probability of $|0\rangle$ by applying U and $U^\dagger$ gates respectively. The $|0\rangle$ probability is measured for each data point with each centroid. Then the data value is assigned to the classified category with the highest probability with the centroid. In the TWTDUS dataset, which contains 8760 entries, the generated system power is divided into two categories using the analytical method (where the nearest value to the generated average power equals 1501.66 KW),

- power generated is more than 1501.66 KW (labeled 1).
- power generated is less than 1501.66 KW (labeled 0).

Similarly, in the SDWTT18 dataset, which consists of 50530 entries, using analytical clustering, the LV active power is divided into two categories based on,

- LV active power is more than 1808.3089599609 KW (labeled 1).
- LV active power is less than 1808.3089599609 KW (labeled 0).

Corresponding to the average generated power, the wind speed (9.52 m/s for the TWTDUS dataset and 8.49664497375488 m/s for the SDWTT18 dataset) is determined. Accordingly, the wind speed is classified into two parts in each dataset individually: (i) a wind speed of more than 9.52 m/s for the TWTDUS dataset and 8.49664497375488 m/s for the SDWTT18 dataset, (ii) a wind speed of less than 9.52 m/s for the TWTDUS dataset and 8.49664497375488 m/s for the SDWTT18 dataset. The centroid point for the two categories (which is calculated based on the nearest value to the average value of the sum of 9.52 m/s and the minimum value of the wind speed, the nearest value to the average value of the sum of 9.52 m/s, and the maximum value of the wind speed, and the same for the SDWTT18 dataset) is selected using the same analytical method. The selected centroid points are already encoded into θ angle of the $U^\dagger$ gate. The wind speed data is encoded into the U gate and the probability of $|0\rangle$ is measured for each data value with the two centroids. The centroid that gives the maximum probability with the data value is accepted. If the maximum probability came from a fixed centroid, then the corresponding data value is labeled 1; otherwise, 0. Hereafter, the result of the power-generated data columns labeled using 0's and 1's are compared to the analytical clustering to get the accuracy of the classification technique. The accuracy is 97.96 % for the TWTDUS dataset and 92.55 % for the SDWTT18 dataset.

2) Variational $UU^\dagger$ Classification

Here, the selected centroids are used, and one layer of the circuit is developed by employing a Hadamard gate, a unitary gate U, a $U^\dagger$ gate, and a second Hadamard. In the case of measuring n layers, n Hadamard gates, n U gates, and the conjugate of these gates, i.e., the mirror image of the initial 2n number of gates, are applied. The dataset's feature values which are mapped from 0 to π, are the θ value of each U gate, and the ϕ and λ values are set to zero. The feature values were selected for each circuit iteration as the θ value of each U gate. The centroid values were set in the θ value $U^\dagger$ gates. The process begins by measuring one layer of the circuit and continues up to 10 layers with a pause of 1 layer for the

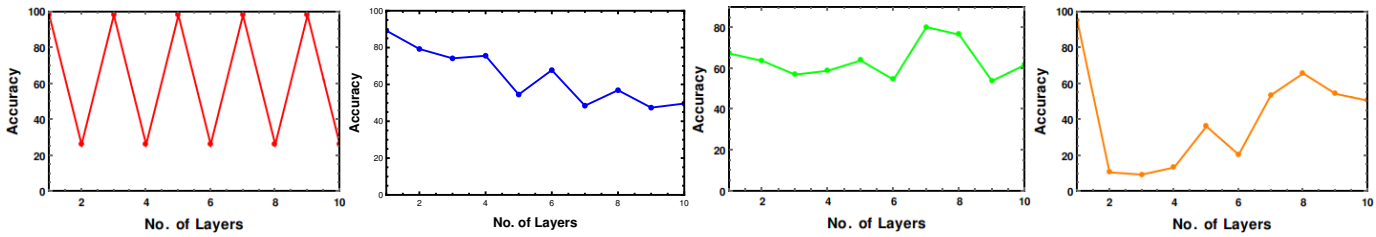

(a) (b) (c) (d)

Fig. 12: The relation of the accuracy versus layers for Variational $UU^{\dagger}$ method using the (a) Analytical method for the TWTDUS dataset, (b) k-Means clustering method for the TWTDUS dataset, (c) Analytical method for the SDWTT18 dataset and (d) k-Means clustering method for the SDWTT18 dataset.

Datasets	Clustering Methods	No. of Layers	Accuracy (%)
TWTDUS	Analytical	1	97.98
		2	26.21
		3	98.08
		4	26.21
		5	98.03
		6	26.21
		7	98.00
		8	26.21
		9	98.10
		10	26.21
TWTDUS	k-Means	1	89.22
		2	79.26
		3	74.16
		4	75.56
		5	54.52
		6	67.77
		7	48.45
		8	56.87
		9	47.39
		10	49.61
SDWTT18	Analytical	1	67.38
		2	63.78
		3	57.04
		4	58.94
		5	63.95
		6	54.58
		7	80.34
		8	76.65
		9	53.93
		10	61.76
SDWTT18	k-Means	1	94.42
		2	10.72
		3	9.49
		4	13.43
		5	36.23
		6	20.57
		7	53.62
		8	65.68
		9	54.35
		10	50.57

TABLE V: Accuracy of each layer of the variational $UU^{\dagger}$ method of classification with analytical and k-Means clustering of the TWTDUS and SDWTT18 datasets.

TWTDUS dataset and the same for the SDWTT18 dataset. The accuracy score of each layer (Table V) is determined such as finding the accuracy in the $UU^{\dagger}$ method of classification, and each data point is assigned to a cluster, i.e., either cluster 0 or cluster 1. If c number of data matches with the analytic method, then accuracy= $\frac{c}{8760(\text{Total number of data})} \times 100$ (as an example, this is for the first dataset.). The accuracy score versus the number of layers for the variational $UU^{\dagger}$ approach using the analytical method for the TWTDUS and SDWTT18 datasets is shown in Fig. 12a and 12c, and using the k-Means clustering method is shown in Fig. 12b and 12d. The best accuracy achieved in layer 9 for the TWTDUS dataset is 98.10% by analytical clustering and 94.42% for the SDWTT18 dataset in layer 1 by k-Means clustering.

3) Simulation of Quantum Neural Network

In both datasets, the input parameters are scaled from 0 to π. Furthermore, training data from 67 % and testing data from 33 % of the dataset are randomly selected. The η value is set to be 0.03, and the input parameters are encoded into the correct qubit state with the appropriate number of qubits (4 qubits for TWTDUS and 2 qubits for SDWTT18) in the circuit, as shown in Fig. 5. Consequently, the qubit states are modified using entangled layers and parameterized rotation gates for a specified number of layers. In this paper, 15 layers are chosen for the TWTDUS dataset and 5 layers for the SDWTT18 dataset due to a lack of computational power. The transformed qubit state is measured using the IBM Qasm simulator by obtaining the expected value of a Hamiltonian operator, such as Pauli gates. These measurements are decoded and converted into relevant output data. The evaluation of the loss function versus epochs for the TWTDUS dataset is shown in Fig. 15a, and the accuracy versus the epochs for this dataset is shown in Fig. 15b. It is apparent that as the number of epochs increases, the loss function is decreased, and the variational circuit is optimized for the training data. Similarly, for the SDWTT18 dataset, the loss versus epochs and accuracy versus epochs are shown in Fig. 15c and Fig. 15d, respectively. It can be observed that the highest accuracy, 91.63%, is achieved for epoch 16 for the TWTDUS dataset and 81.32% for the SDWTT18 dataset for epoch 2.

4) Noise models

Various types of noise in a quantum system (bit-flip, phase-flip, depolarizing, amplitude damping, and phase damping) were applied to the two datasets and the accuracy deviation was compared. The probability of noise errors has been varied from η = 0 to 1, with an interval of 0.1. The accuracy vs noise model of the TWTDUS and SDWTT18 datasets for $UU^{\dagger}$ using analytical clustering, $UU^{\dagger}$ using k-Means clustering, variational $UU^{\dagger}$ using analytical clustering, and variational $UU^{\dagger}$ using k-Means clustering are shown in Fig. 13 and 14, respectively. Obviously, for the $UU^{\dagger}$ using both analytical and k-Means clustering methods, a general tendency is that

the bitflip noise model shows a sharp decline in accuracy with increasing the probability of the noise parameter (η). Furthermore, the depolarizing and amplitude-damping noise model shows a decreasing accuracy tendency with increasing noise parameter probability. However, the phase-flip and phase-damping models show little to no effect on accuracy with increasing the noise parameter probability. Unfortunately, we cannot draw any conclusive observations for the variational $UU^\dagger$ circuits of analytical and k-Means clustering since all the noise models show no particular trend.

Datasets	Clustering Methods	Classification Methods	Accuracy (%)
TWTDUS Dataset	Analytical	$UU^\dagger$	97.96
		Variational $UU^\dagger$	98.10
	k-Means	$UU^\dagger$	87.69
		Variational $UU^\dagger$	89.22
		QNN	91.63
SDWTT18 Dataset	Analytical	$UU^\dagger$	92.55
		Variational $UU^\dagger$	80.34
	k-Means	$UU^\dagger$	94.43
		Variational $UU^\dagger$	89.22
		QNN	81.32

TABLE VI: Experimental quantum results of all methods of classification.

Datasets	Classification Methods	Accuracy (%)
TWTDUS Dataset	Linear regression	91.10
	KNeighborsRegressor	93.18
	Support vector regression	-6.92
SDWTT18 Dataset	Linear regression	83.37
	Descision tree regressor	83.72
	Support vector regression	-0.17

TABLE VII: Experimental classical results of all methods of classification.

V. Discussion and Conclusion

IoT systems are being deployed in various applications with unique requirements. Extreme events such as extreme temperatures, winds, flooding, and snow storms can adversely affect the infrastructure and IoT systems. Therefore, it is essential to assess damage effectively and with minimal manual involvement to minimize service degradation, maximize coverage, and optimize the services offered. Additionally, extreme heterogeneity in population and wealth distribution and associated demographic, socio-economic, and business considerations must be considered.

In this paper, we proposed a classical-quantum hybrid system to efficiently cluster and classify IoT extreme events. Two classical clustering methods; the analytical and k-Means are used to cluster the dataset into two groups classically. In the analytical method, the dataset is divided into two categories (i) from minimum to average of the maximum and minimum power generated, (ii) from the average of the maximum and minimum power generated to maximum power generated. k-Means is an unsupervised learning algorithm; it divides the data points into two clusters based on the minimum Euclidean distance from the cluster centroids. After the clusters' centroids were obtained using classical methods, the datasets were encoded along with their features into a quantum circuit to obtain prediction accuracy of various quantum algorithms. Here, three types of quantum algorithms for data classification are used: $UU^\dagger$ classifier, Variational $UU^\dagger$ classifier, and Quantum Neural Network (QNN).

For the $UU^\dagger$ method, a single data feature is encoded in U, and a centroid point corresponds to the data feature in $U^\dagger$. Then the inner product with $UU^\dagger$ is calculated for each centroid, and the cluster is assigned to each data point based on the highest value of the inner product with each centroid. This is compared with the classical clustering methods to compute the accuracy. The same approach is applied in the variational $UU^\dagger$ method but with more qubits and numerous layers to encode all the data features. The QNN method comprises variational circuits that use rotation gates to encode and approximate a unitary operation on quantum states. The variational circuit aims to minimize the cost function for a given learning model by updating the gradient after each iteration until the cost function is minimized. The learning model after the cost function minimization provides the desired solution. It is shown from Table VI that the accuracy for $UU^\dagger$, variational $UU^\dagger$ classification with analytical clustering is 97.96% and 98.10%, respectively. The accuracy for $UU^\dagger$, variational $UU^\dagger$ classification with k-Means clustering is 87.69% and 89.22%, respectively. While the accuracy for QNN without any pre-clustering is 91.63%. The $UU^\dagger$, variational $UU^\dagger$ classification with analytical clustering provides perfect prediction accuracy in all the above methods. Therefore, our proposed classical-quantum hybrid model achieves outstanding prediction accuracy compared to the classical methods (Tables VI and VII) and under Noisy Intermediate Scale Quantum (NISQ) era.

However, the maximum quantum speedup still needs to be achieved due to the one-to-one encoding of classical information into quantum systems. The proposed model has two main advantages against the classical methods: first, the classical techniques require a large space to store and manipulate the dataset, whereas, in quantum methods, only a small number of qubits is needed. Secondly, the accuracy of quantum methods (especially $UU^\dagger$) for both datasets is much higher than comparing the classical techniques. The proposed classification techniques can be extended to classify datasets having a large number of features into different categories for energy utilization and conservation of the IoT systems in extreme environments. This will open new approaches to forecast output power generation daily, save energy waste and costs in an IoT-extreme environment and provide accurate

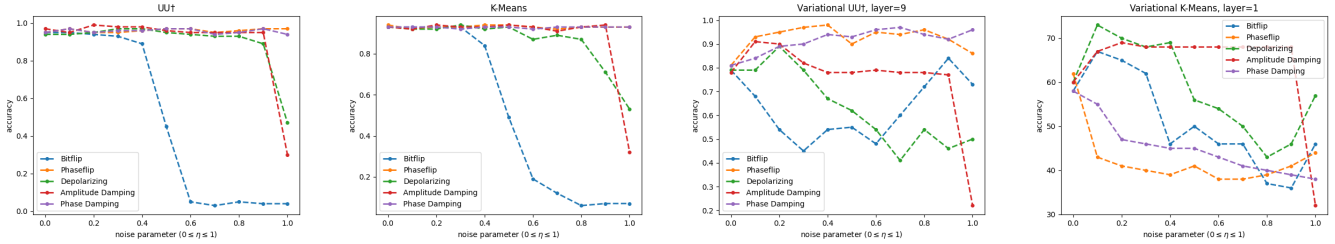

(a) (b) (c) (d)

Fig. 13: Accuracy vs Noise parameters of the TWTDUS dataset for (a) $UU^\dagger$ using analytical clustering, (b) $UU^\dagger$ using k-Means clustering, (c) Variational $UU^\dagger$ using analytical clustering, layer=9 and (d) Variational $UU^\dagger$ using k-Means clustering, layer=1. Noise parameter η is taken from 0 to 1 with an increment of 0.1.

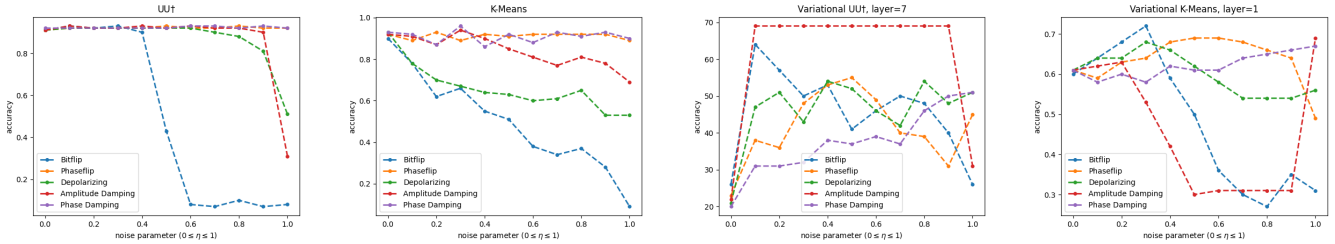

(a) (b) (c) (d)

Fig. 14: Accuracy vs Noise parameters of the SDWTT18 dataset for (a) $UU^\dagger$ using analytical clustering, (b) $UU^\dagger$ using k-Means clustering, (c) Variational $UU^\dagger$ using analytical clustering, layer=7 and (d) Variational $UU^\dagger$ using k-Means clustering, layer=1. Noise parameter η is taken from 0 to 1 with an increment of 0.1.

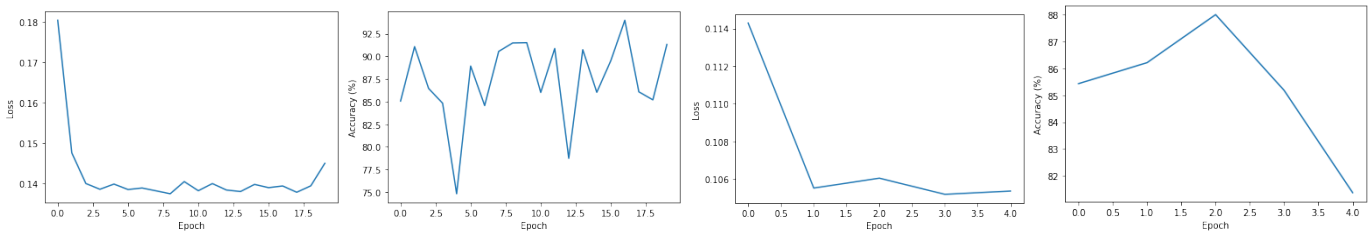

(a) (b) (c) (d)

Fig. 15: Quantum Neural Network(QNN). (a) Relation of loss function versus epochs for the TWTDUS, (b) Relation of accuracy versus epochs for the TWTDUS, (c) Relation of loss function versus epochs for the SDWTT18, (d) Relation of accuracy versus epochs for the SDWTT18.

decision-making in the energy sector.

REFERENCES

[1] M. Nielsen and I. Chuang, *Quantum Computation and Quantum Information*, 2010. [Online]. Available: http://mmrc.amss.cas.cn/tlb/201702/W020170224608149940643.pdf

[2] A. W. Harrow and A. Montanaro, "Quantum computational supremacy," *Nature*, vol. 549, p. 203, 2017. [Online]. Available: http://mmrc.amss.cas.cn/tlb/201702/W020170224608149940643.pdf

[3] T. F. Rønnow, Z. Wang, J. Job, S. Boixo, S. V. Isakov, D. Wecker, J. M. Martinis, D. A. Lidar, and M. Troyer, "Defining and detecting quantum speedup," *Science*, vol. 345, no. 6195, pp. 420–424, 2014. [Online]. Available: https://www.science.org/doi/abs/10.1126/science.1252319

[4] S. Boixo, S. Isakov, V. Smelyanskiy, R. Babbush, N. Ding, Z. Jiang, M. J. Bremner, J. Martinis, and H. Neven, "Characterizing quantum supremacy in near-term devices," *Nature Physics*, vol. 14, p. 595–600, 2018. [Online]. Available: https://www.nature.com/articles/s41567-018-0124-x

[5] P. Shor, "Algorithms for quantum computation: discrete logarithms and factoring," in *Proceedings 35th Annual Symposium on Foundations of Computer Science*, 1994, pp. 124–134. [Online]. Available: https://ieeexplore.ieee.org/document/365700

[6] L. K. Grover, "A fast quantum mechanical algorithm for database search," in *ANNUAL ACM SYMPOSIUM ON THEORY OF COMPUTING*. ACM, 1996, pp. 212–219. [Online]. Available: https://arxiv.org/abs/quant-ph/9605043

[7] N. Abdelgaber and C. Nikolopoulos, "Overview on quantum computing and its applications in artificial intelligence," in *2020 IEEE Third International Conference on Artificial Intelligence and Knowledge Engineering (AIKE)*, 2020, pp. 198–199. [Online]. Available: https://ieeexplore.ieee.org/document/9355449

[8] Y. Cao, J. Romero, J. P. Olson, M. Degroote, P. D. Johnson, M. Kieferová, I. D. Kivlichan, T. Menke, B. Peropadre, N. P. D. Sawaya, S. Sim, L. Veis, and A. Aspuru-Guzik, "Quantum chemistry in the age of quantum computing," *Chemical Reviews*, vol. 119, no. 19, pp. 10 856–10 915, 2019, pMID: 31469277. [Online]. Available: https://doi.org/10.1021/acs.chemrev.8b00803

[9] R. Orús, S. Mugel, and E. Lizaso, "Quantum computing for finance: Overview and prospects," *Reviews in Physics*, vol. 4, p. 10028, 2019. [Online]. Available: https://doi.org/10.1016/j.revip.2019.100028

[10] Y. Cao, J. Romero, and A. Aspuru-Guzik, "Potential of quantum computing for drug discovery," *IBM J. Res. Dev.*, vol. 62, no. 6, nov 2018. [Online]. Available: https://doi.org/10.1147/JRD.2018.2888987

[11] A. V. Frolov, "Can a quantum computer be applied for numerical

weather prediction?" *Russ. Meteorol. Hydrol.*, vol. 42, p. 545–553, 2017. [Online]. Available: https://doi.org/10.3103/S1068373917090011

[12] A. J.-A. et al., "Optimized surface code communication in superconducting quantum computers," *Proceedings of the 50th Annual IEEE/ACM International Symposium on Microarchitecture*, vol. 42, 2020. [Online]. Available: https://doi.org/10.3103/S1068373917090011

[13] N. Laxminarayana, N. Mishra, P. Tiwari, S. Garg, B. K. Behera, and A. Farouk, "Quantum-assisted activation for supervised learning in healthcare-based intrusion detection systems," *IEEE Transactions on Artificial Intelligence*, 2022. [Online]. Available: https://ieeexplore.ieee.org/abstract/document/9813378

[14] S. Deshmukh, B. K. Behera, P. Mulay, E. A. Ahmed, S. Al-Kuwari, P. Tiwari, and A. Farouk, "Explainable quantum clustering method to model medical data," *Knowledge-Based Systems*, vol. 267, p. 110413, 2023. [Online]. Available: https://www.sciencedirect.com/science/article/abs/pii/S0950705123001636

[15] "Eia projects nearly 50% increase in world energy usage by 2050," 2019. [Online]. Available: https://www.eia.gov/todayinenergy/detail.php?id=41433

[16] M. Hightower and S. Pierce, "The energy challenge," *Nature*, vol. 452, pp. 285–286, 2008. [Online]. Available: https://doi.org/10.1038/452285a

[17] B. Muruganantham, R. Gnanadass, and N. Padhy, "Challenges with renewable energy sources and storage in practical distribution systems," *Renewable and Sustainable Energy Reviews*, vol. 73, pp. 125–134, 2017. [Online]. Available: https://doi.org/10.1016/j.rser.2017.01.089

[18] R. Zafar and A. M. et al., "Prosumer based energy management and sharing in smart grid, renewable and sustainable energy reviews," *Renewable and Sustainable Energy Reviews*, vol. 82, pp. 1675–1684, 2018. [Online]. Available: https://doi.org/10.1016/j.rser.2017.07.018

[19] A. Ajagekar and F. You, "Quantum computing for energy systems optimization: Challenges and opportunities," *Energy*, vol. 179, pp. 76–89, 2019. [Online]. Available: https://doi.org/10.1016/j.energy.2019.04.186

[20] A. B. et al., "Challenges in the smart grid applications: an overview," *International Journal of Distributed Sensor Networks*, vol. 10, no. 2, p. 974682, 2014. [Online]. Available: https://doi.org/10.1016/j.energy.2019.04.186

[21] D. C. Cafaro and I. E. Grossmann, "Strategic planning, design, and development of the shale gas supply chain network," *AIChE Journal*, vol. 60, no. 6, pp. 2122–2142, 2014. [Online]. Available: https://doi.org/10.1016/j.energy.2019.04.186

[22] e. a. V. Hassija, "Present landscape of quantum computing," *IET Quantum Communication*, vol. 1, no. 2, pp. 42–48, 2020. [Online]. Available: https://doi.org/10.1016/j.energy.2019.04.186

[23] P. J. Denning and T. G. Lewis, "Exponential laws of computing growth," *Communications of the ACM*, vol. 60, no. 1, pp. 54–65, 2017. [Online]. Available: https://dl.acm.org/doi/10.1145/2976758

[24] A. Ajagekar and F. You, "Quantum computing and quantum artificial intelligence for renewable and sustainable energy: A emerging prospect towards climate neutrality," *Renewable and Sustainable Energy Reviews*, vol. 112493, pp. 1364–0321, 2022. [Online]. Available: https://doi.org/10.1016/j.rser.2022.112493

[25] J. Tangpanitanon, "Quantum computing for energy system optimisation," *Quantum Technology Foundation*, 2020. [Online]. Available: https://www.qtft.org/post/copy-of-the-hottest-apps-on-the-market

[26] N. Nikmehr, P. Zhang, and M. Bragin, "Quantum distributed unit commitment," *IEEE Transactions on Power Systems*, 2022. [Online]. Available: https://doi.org/10.1109/TPWRS.2022.3141794

[27] L. Cochrane, D. S. Jordan, and D. B. Lackey, "Quantum impact: Energy and utilities," 2020. [Online]. Available: https://azure.microsoft.com/en-us/resources/quantum-impact-energy-and-utilities-/

[28] Q. Alqarqaz, "How microsoft could redefine the power industry with quantum computing," *BINUS UNIVERSITY COMPUTER ENGINEERING*, 2021. [Online]. Available: https://spectrum.ieee.org/how-microsoft-could-redefine-the-power-industry-with-quantum-computing

[29] M. Reiher and N. W. et al., "Elucidating reaction mechanisms on quantum computers," *Proceedings of the National Academy of Sciences*, 2017. [Online]. Available: https://spectrum.ieee.org/how-microsoft-could-redefine-the-power-industry-with-quantum-computing

[30] Q. Gao and H. Nakamura, "Computational investigations of the lithium superoxide dimer rearrangement on noisy quantum devices," *arXiv:1906.10675*, 2019. [Online]. Available: https://doi.org/10.48550/arXiv.1906.10675

[31] F. Tavares, "Google and nasa achieve quantum supremacy, nasa's ames research center," 2019. [Online]. Available: https://www.nasa.gov/feature/ames/quantum-supremacy

[32] D. Aloise, A. Deshpande, and P. H. et al., "Np-hardness of euclidean sum-of-squares clustering," *Mach Learn*, vol. 75, p. 245–248, 2009. [Online]. Available: https://doi.org/10.1007/s10994-009-5103-0

[33] V. Kumar, G. Bass, C. Tomlin, and J. Dulny, "Quantum annealing for combinatorial clustering," *Quantum Information Processing*, vol. 17, no. 2, p. 1–14, feb 2018. [Online]. Available: https://doi.org/10.1007/s11128-017-1809-2

[34] D. Arthur and P. Date, "Balanced k-means clustering on an adiabatic quantum computer," *Quantum Information Processing*, vol. 20, no. 9, sep 2021. [Online]. Available: https://doi.org/10.1007/s11128-021-03240-8

[35] N. Mohanty, B. K. Behera, and C. Ferrie, "Analysis of the vehicle routing problem solved via hybrid quantum algorithms in presence of noisy channels," *arXiv preprint ll oharXiv:2205.07630*, 2022. [Online]. Available: https://arxiv.org/abs/2205.07630

[36] C. Bauckhage, E. Brito, K. Cvejoski, C. Ojeda, R. Sifa, and S. Wrobel, "Ising models for binary clustering via adiabatic quantum computing," in *Energy Minimization Methods in Computer Vision and Pattern Recognition*, M. Pelillo and E. Hancock, Eds. Cham: Springer International Publishing, 2018, pp. 3–17. [Online]. Available: https://www.springerprofessional.de/ising-models-for-binary-clustering-via-adiabatic-quantum-computi/15558034

[37] K. Benlamine, Y. Bennani, N. Grozavu, and B. Matei, "Quantum collaborative k-means," 07 2020, pp. 1–7. [Online]. Available: https://ieeexplore.ieee.org/document/9207334

[38] I. Kerenidis, J. Landman, A. Luongo, and A. Prakash, "q-means: A quantum algorithm for unsupervised machine learning," 2018. [Online]. Available: https://arxiv.org/abs/1812.03584

[39] S. U. Khan, A. J. Awan, and G. Vall-Llosera, "K-means clustering on noisy intermediate scale quantum computers," 2019. [Online]. Available: https://arxiv.org/abs/1909.12183

[40] S. Johri, S. Debnath, A. Mocherla, A. Singh, A. Prakash, J. Kim, and I. Kerenidis, "Nearest centroid classification on a trapped ion quantum computer," 2020. [Online]. Available: https://arxiv.org/abs/2012.04145

[41] S. Diadamo, C. O'Meara, G. Cortiana, and J. Bernabe-Moreno, "Practical quantum k-means clustering: Performance analysis and applications in energy grid classification," *IEEE Transactions on Quantum Engineering*, pp. 1–16, 2022. [Online]. Available: https://arxiv.org/abs/2112.08506

[42] Y. Kwak, W. J. Yun, S. Jung, and J. Kim, "Quantum neural networks: Concepts, applications, and challenges," 2021. [Online]. Available: https://arxiv.org/abs/2108.01468

[43] A. Macaluso, L. Clissa, S. Lodi, and C. Sartori, "A variational algorithm for quantum neural networks," pp. 591–604, 2020.

[44] D. Singh, S. Kumar, and B. K. Behera, "Complexity analysis of quantum teleportation via different entangled channels in the presence of noise," *IET Quantum Communication*, vol. 4, no. 1, pp. 1–16, 2023. [Online]. Available: https://ietresearch.onlinelibrary.wiley.com/doi/abs/10.1049/qtc2.12048